Albert-Einstein-Institut
Hannover

LIGO

August 9, 2013

Control loop design for the aLIGO second loop power stabilization

LIGO-NUMBER

Jan Hendrik Põld (jan.poeld@aei.mpg.de), Peter King, Benno Willke

This documents gives an overview of the tests and design of the aLIGO second loop power stabilization. It focuses on the design of the control loop and the question whether it is possible to build a digital control loop.

Max-Planck-Institute for Gravitational Physics
Albert-Einstein-Institute
Callinstrasse 38
30167 Hannover

California Institute of Technology
LIGO Project, MS 18-34
1200 E. California Blvd.
Pasadena, CA 91125

Contents

1 Introduction

This document reviews tests for the second loop power stabilization that were done at LLO. Based on the results and simulations we propose a final design for the second loop servo electronics. A schematic overview of the aLIGO power stabilization is shown in Fig.1.

It consists of a first and a second loop. The first loop is used as pre-stabilization in order to reach a power noise level of $2 \cdot 10^{-8}/\sqrt{\text{Hz}}$ at 10 Hz. The sensing is done downstream of the Pre-Modecleaner and the control signal is fed back to an AOM. However, the interferometer requires a beam with a power stability of $2 \cdot 10^{-9}/\sqrt{\text{Hz}}$ 10 Hz at full input power of 125 W and therefore a second sensor is placed inside the vacuum system downstream of the Input-Modecleaner (IMC). The control signal of the second loop is fed back into the error point of the first loop.

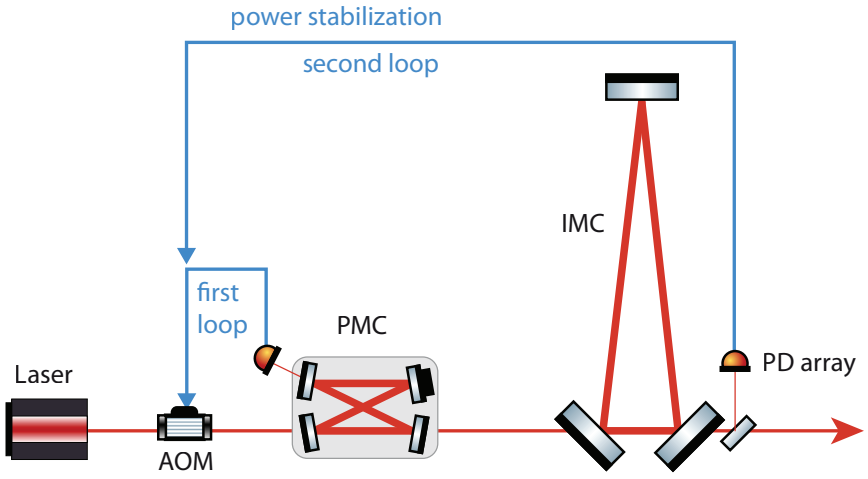

Figure 1: Schematic overview of aLIGO power stabilization

2 Hardware

The photodiode (PD) array (see Fig.2 and D1101059 PD assembly) consists of four in-loop and four out-of-loop sensors in order to sense a total photo current up to 250 mA. The beam put into the PD array is split by a 50:50 beam splitter and directed towards two levels. Each of these beams is further split into four beams on each level (see Fig. 3) and hits the sensor (Excelitas (former Perkin Elmer) C30642) under a 45 degree angle. BG39 filters are used to absorb residal light that is reflected off the PD chip.

The PDs are mounted in isolated aluminum cans that can be adjusted horizontally and vertically to position the input beam onto the PDs. During initial alignment those PDs are optimized to have a minimum pointing to power noise coupling.

To further monitor the beam position and measure the pointing noise a small fraction of the beam is sensed with a quadrant detector (FCI InGaAs-Q3000) that is also part of the PD array.

For the readout circuit boards are mounted to the back of the PDs and coaxial in-vacuum cables (D1200280-v1 aLIGO PSL ISS PD Coax Cable) are used to connect the signal to the vacuum feedthrough. The feedthrough used at LLO is LHAM2-D2 (D1002885 HAM2 flange layout) and WHAM2-D5 at LHO. Thus the in-vacuum cable length for LHO is 108 inch and for LLO 192 inch to reach the flange.

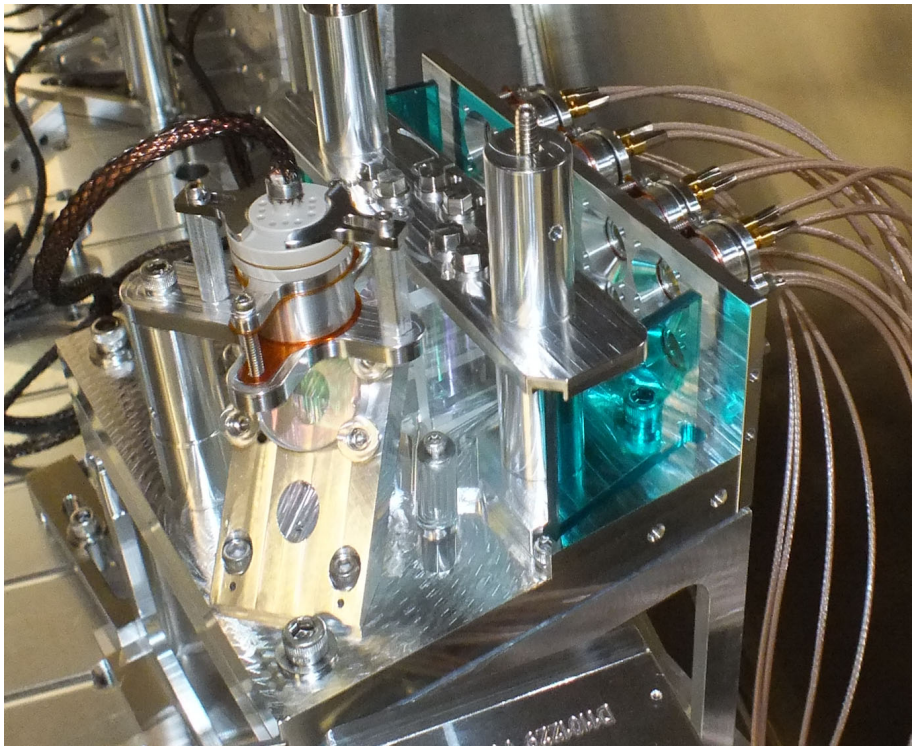

Figure 2: Picture of PD array

2.1 Modifications

Due to the experiences (more information on this topic: LLO alog 5955: status of PD array and LLO alog 6566: PD array was taken out of HAM2) we made with the first version of the array at LLO modifications are necessary to make the PD array more robust. The modifications are listed in LIGO-E1300122 (Advanced LIGO Engineering Change Request (ECR) - ISS PD Array (BUG 71)) and were discussed at the PSL Outer Loop Power Stabilization Delta Final Design Review (LIGO-T1300192-v1).

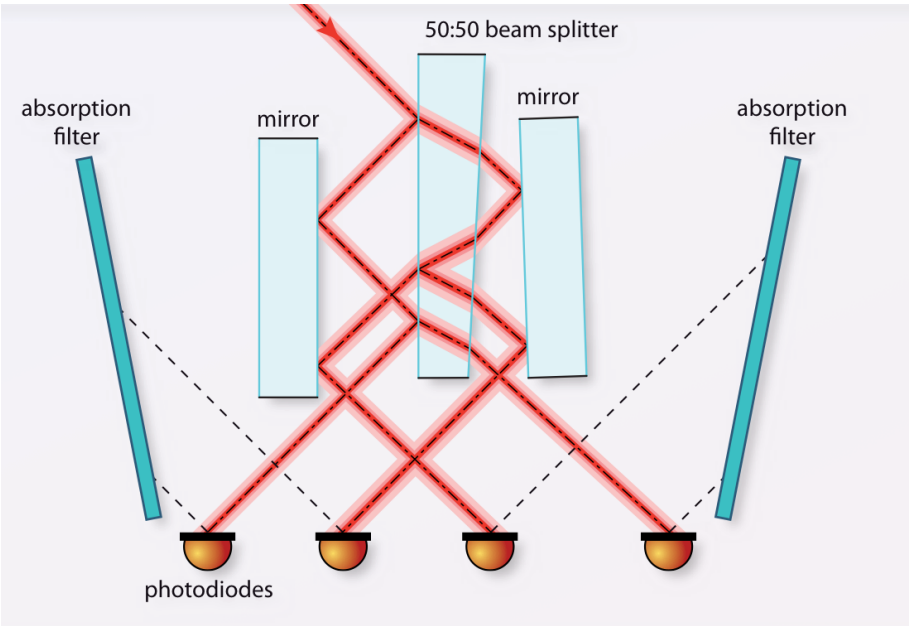

Figure 3: Optical path

2.2 Alignment

Information on alignment and modematching can be found in [1]. The beam radius on the PDs is about 550 μm. No performance difference was found for beam radii between 60 μm to 720 μm in a prior experiment [2].

3 Free running power noise

The first loop power stabilization sensor is downstream of the Pre-Modecleaner (PMC) and the shot noise limited performance is at a level of $2 \cdot 10^{-8}/\sqrt{\text{Hz}}$ for frequencies between 10Hz and 1kHz. We measured excess power noise at the bottom of the periscope at the end of the pre-stabilized laser (PSL)/ input optics (IO) table, in reflection of the Input-Modecleaner (IMC) while it was misaligned and not locked and in transmission of the IMC (see Fig. 4).

In comparison to the LLO results the noise curve measured at LHO in transmission of IM4 is even worse, especially at low frequencies. This is most likely due to the influence of the HEPA fans that were running in the laser room at the time of the measurement (LHO alog 6369: RIN of MC transmission). It was recently discovered that a fair amount of power noise measured downstream of the IMC is due to pointing noise to power noise conversion. The high pointing noise was traced back to a noisy control loop that drives the steering PZT on the top of the periscope (LLO alog 6446: summary on IMC beam jitter).

Since the IMC was not available at this time the results were a projection based on a measurement on the PSL/IO table. For the analysis two scenarios will therefore be assumed. One worst case that assumes the free running power noise measured with IM4 trans QPD and another case that takes the power noise measured in reflection of the IMC, assuming that the pointing to power noise contribution downstream the IMC is below a power noise of $1 \cdot 10^{-6} / \sqrt{\text{Hz}}$.

Further investigation showed that the noise came close to the level that was measured in reflection of the IMC (LLO alog 7676: IMC RIN).

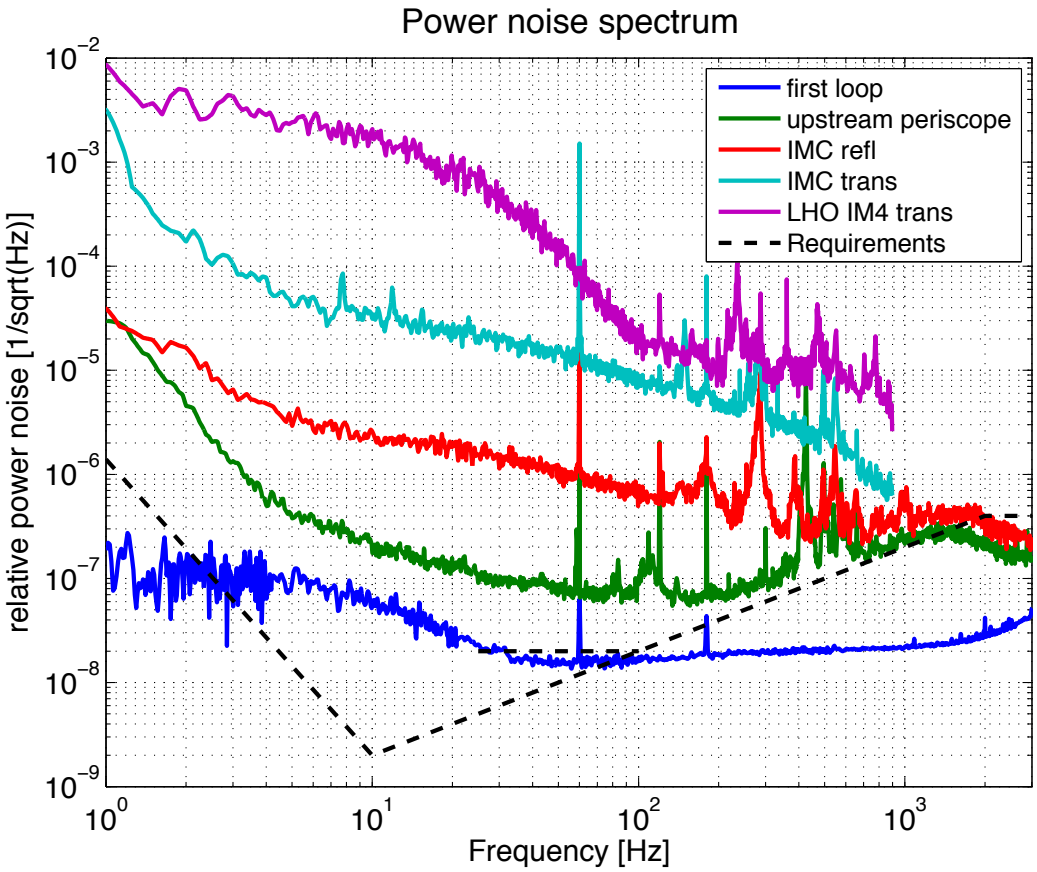

Figure 4: Free running power noise

3.1 Pointing noise coupling and QPD readout

Since the optical response of a photo detector is also sensitive to pointing the tolerable pointing noise at the array is shown in figure 5. A coupling factor of 10/m is assumed which should be achievable based on prior experience [3][4], because the PD array is optimized for minimum pointing coupling.

The expected photocurrent on the QPD is 100 μA with 125 W at the interferometer input. Therefore we recommend to change the transimpedance resistor in the QPD transimpedance amplifier to 100 kΩ (LLO alog 7448: ISS array alignment).

As the QPD is not in the same plane as the eight PDs used for the power stabilization, it can not serve as reference in the current setup [1].

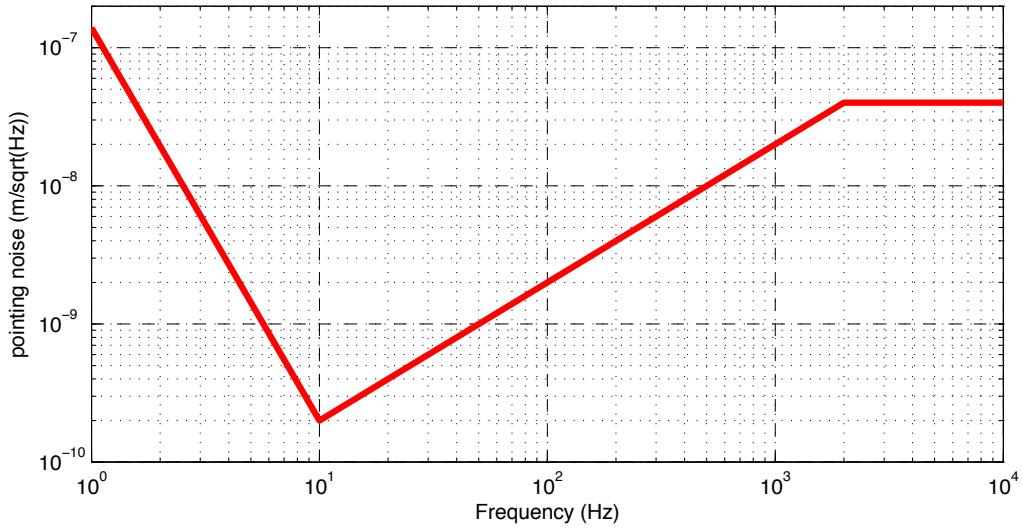

Figure 5: Estimated tolerable pointing noise on array QPD

4 Control loop design

The power noise downstream of the IMC was expected not to exceed $1 \cdot 10^{-7}/\sqrt{Hz}$ above a Fourier frequency of 10 Hz. So far the approach was a digital control loop with the advantage of changing filter modules on the fly (LIGO-L1100279: Review Report on the PSL Outer Loop Power Stabilization Final Design, T1100265-v1 Outer Loop Power Stabilisation Final Design). However, as discussed in the previous section the actual power noise is higher than expected. To get a good estimate for the loop shape and the cross over to the first loop, a Simulink model was set up (Fig.6).

4.1 Actuator transfer function

The aLIGO power stabilization consists of a nested control loop (Fig.1 and Fig.6). It has two sensors, one single PD on the PSL table and the PD array in HAM2. An AOM is used as actuator. The control signal from the second loop is injected into the error point of the first loop.

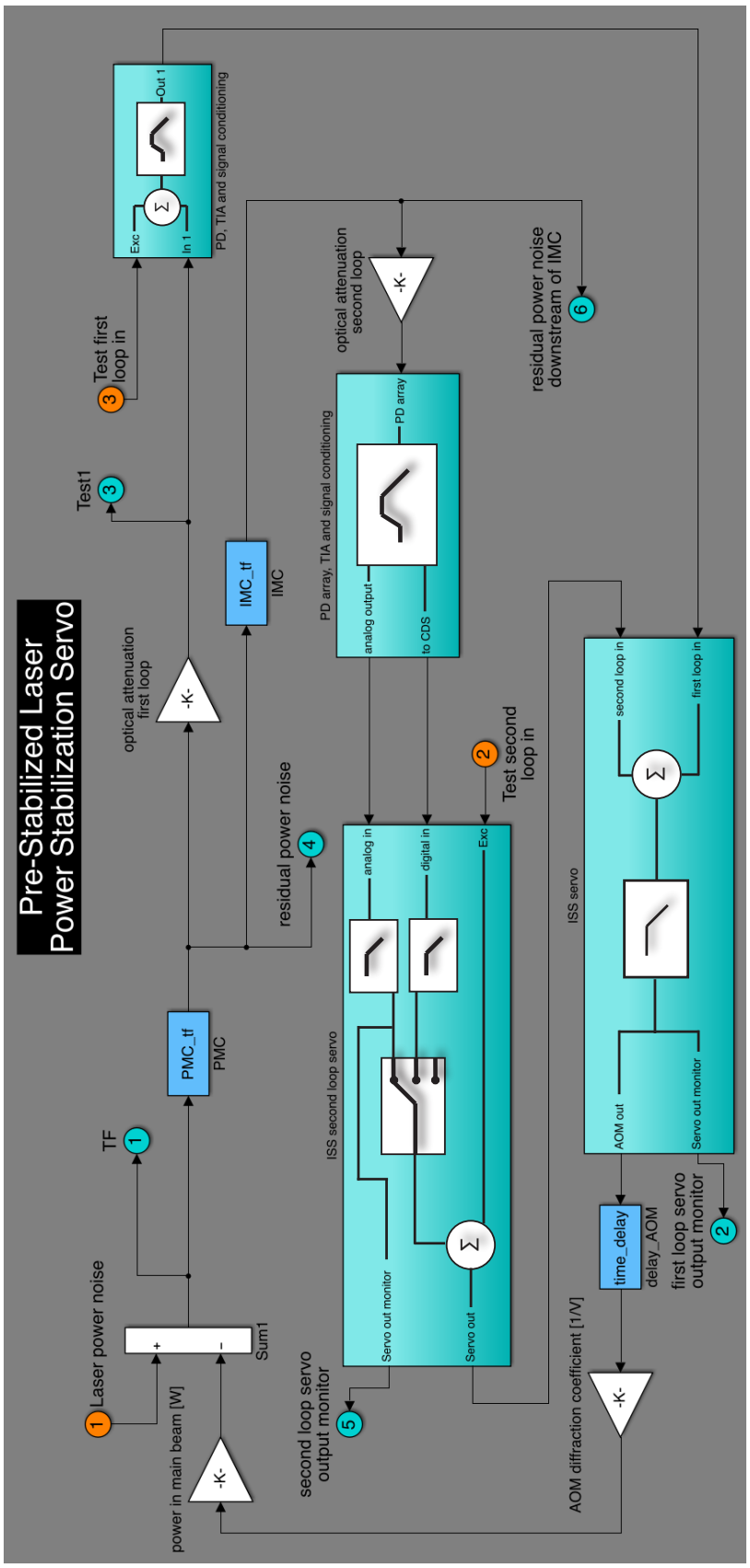

Figure 6: Schematic overview of Simulink model

To obtain the actuator transfer function of the servo loop, a signal is injected into the error point of the first loop and the response is measured at the PD array. Since the PD array was not installed at the time of the measurement, the out-of-loop PD of the first loop was used to measure the response. It was calibrated and projected with the Simulink model to output port 4 (Fig.6).

Figure 7 shows a comparison of the simulated second loop actuator transfer function with the measured one and a simulation of the transfer function including the IMC. The difference between the two projections is the influence of the IMC power noise filtering above its pole frequency of 8721 Hz. Amplitude and phase of the measurement agree very well with the model up to 10 kHz.

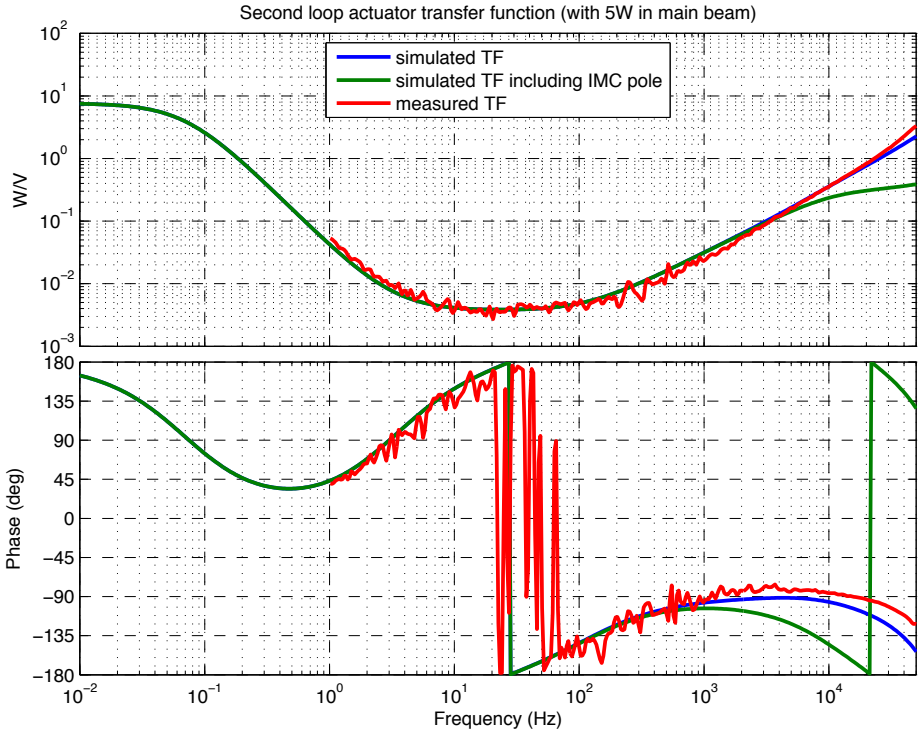

Figure 7: Second loop actuator transfer function

4.2 Experience with the second loop at LLO

A first PD array was installed at LLO in October 2012. As mentioned earlier, mechanical and PD readout problems made it impossible to use the PD array as second loop sensor. Instead a 3 mm Perkin Elmer PD (C30665) was set up in transmission of the IMC (on IOT2L) and used as in-loop sensor. The quadrant in vacuum photodetector that is monitoring the transmitted light of IM4 was used for the out-of-loop measurement.

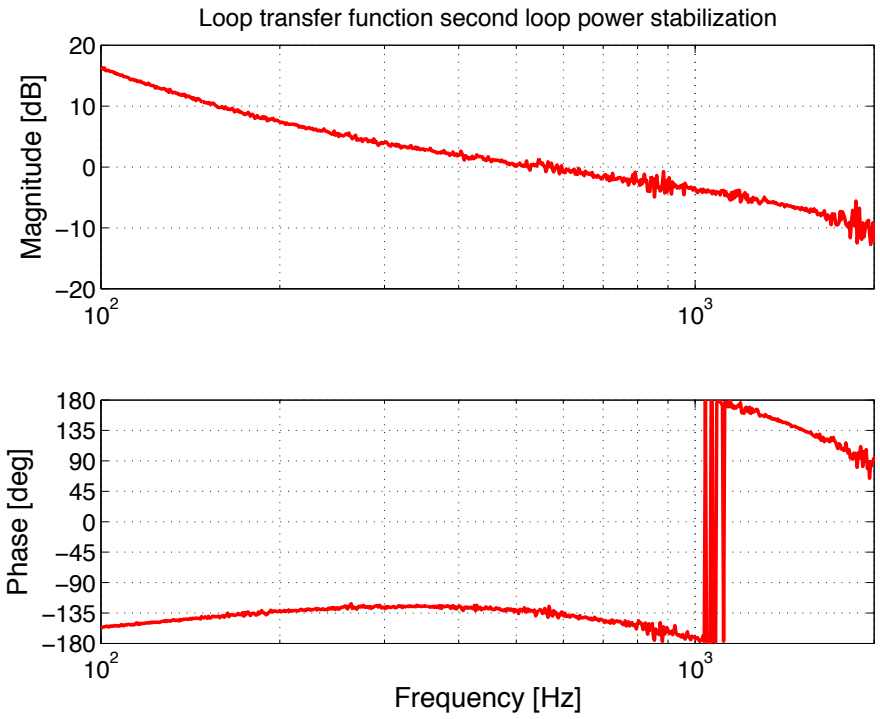

Figure 8: Transfer function of digital loop

The PD signal was whitened and then sampled with the CDS system. The servo consisted of three poles at 1 Hz, 5 Hz and 10 Hz and two zeroes at 50 Hz and 200 Hz. For the feedback to the error point of the first loop the Inputtransfer2 input on the ISS electronics was used and R57 changed to 1 kHz to provide more dynamic range. The transfer function of the second loop is shown in figure 8. It provides a unity gain frequency of 600 Hz with a 45 degree phase margin (LLO alog 5993: performance of second loop with in loop detector on ISC table).

The bandwidth was limited by the 32 kHz sampling rate of the real time model and the anti-aliasing filters (LLO alog 5420: loopback test). It is possible to increase the sampling rate of the real time model to 65 kHz.

Looking at the in-loop measurement (Fig.9) the noise is suppressed to a level of $1 \cdot 10^{-7}/\sqrt{Hz}$ at 10 Hz. However, this result could not be confirmed by the out-of-loop measurement, since it was dominated by electronics noise. As the unity gain frequency is only 600 Hz the in-loop performance was loop gain limited. While the second loop was closed there were no instabilities of the first loop error point.

A first measurement of the second loop using the PD array as sensor was done recently and documented in LLO alog 8031.

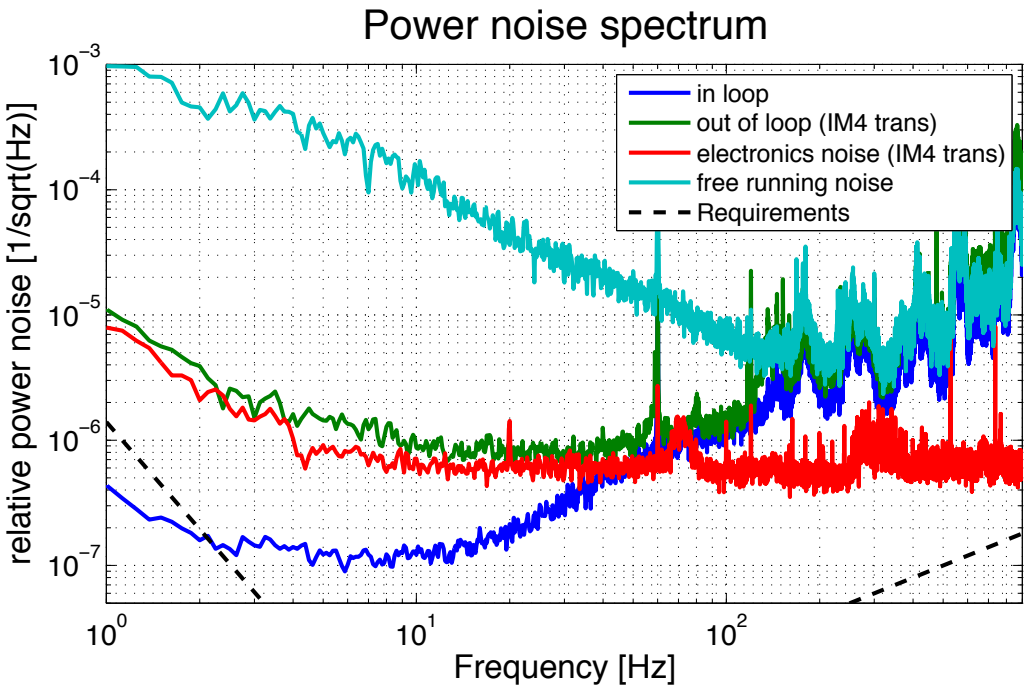

Figure 9: Relative power noise spectrum of digital loop

4.3 Proposed control loop

The experiences from the LLO test reveal that it is not possible to reach the anticipated power stability with a digital control loop with the current noise level downstream of the IMC. Hence, the proposed loop design will use an analog servo electronics.

4.3.1 Signal chain

The proposed signal chain is shown on page 5 of T1100265-v1 (Outer Loop Power Stabilisation Final Design). However the scheme used is slightly modified as shown in figure 10, since the signal conditioning filter and the second loop servo electronics are not located in the same rack, the signal will be transmitted differentially.

4.3.2 Signal conditioning filter

For the readout of the array PDs a low noise transimpedance amplifier in combination with a signal conditioning filter is used (D1300247 Signal conditioning filter layout). This electronics is located close to the vacuum chamber feedthrough.

A LISO simulation of the transfer function of the signal conditioning electronics including a zero-pole fit is shown in figure 11 and table 1. Furthermore, a simulation of the input referred current noise (Fig.12) was conducted with two different transimpedance resistors. It indicates that the electronics noise level is well below the shot noise of 20 mA

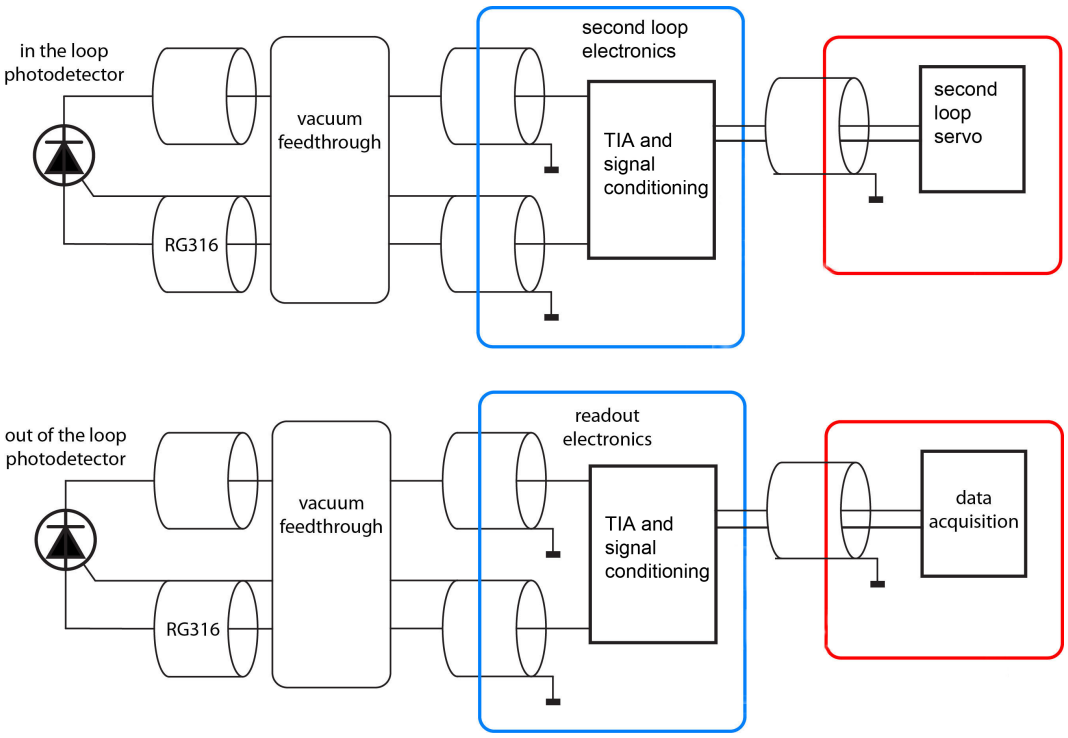

Figure 10: Signal chain

detected photo current for 125W input power to the interferometer which corresponds to $8 \cdot 10^{-11} \mathrm{A}/\sqrt{Hz}$. According to the simulation, the electronics noise of the circuit will dominate the quantum noise at 10 Hz if the interferometer input power is less than 1W. If the interferometer will be operated at less input power than 125 W for a long time, the transimpedance resistor will be adjusted such that there are ~10 V at the output of the TIA. At an interferometer input power of 125 W the transimpedance resistor is 330 Ω. However, this has to be verified by a measurement, since the measured noise has been up to an order of magnitude higher than the LISO simulation in previous experiments [2].

4.3.3 Control loop shape

A Simulink model was developed to simulate the loop transfer functions of the first and second loop. The unity gain frequency of the second loop is at 4 kHz with a phase margin of 80 degree (Fig.13). At 10 Hz the gain of the second loop is 78 dB (Fig.14). The unity

zero	6.6 mHz	70.7 mHz		
pole	3.23 Hz	3.11 Hz	116.6 Hz	24.65 kHz
gain	0.102			

Table 1: Poles and zeros of second loop signal conditioning filter

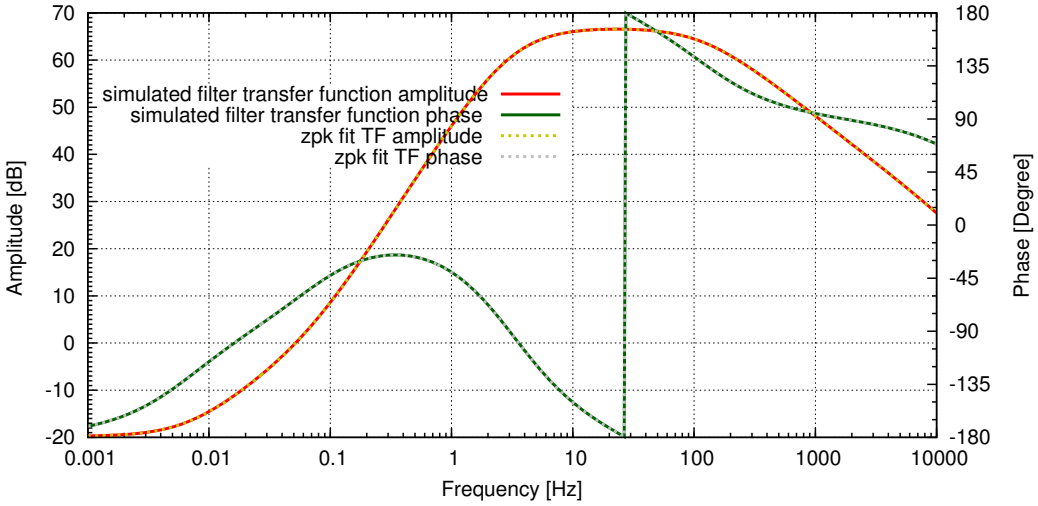

Figure 11: LISO simulation of signal conditioning filter transfer function and fit of poles and zeroes

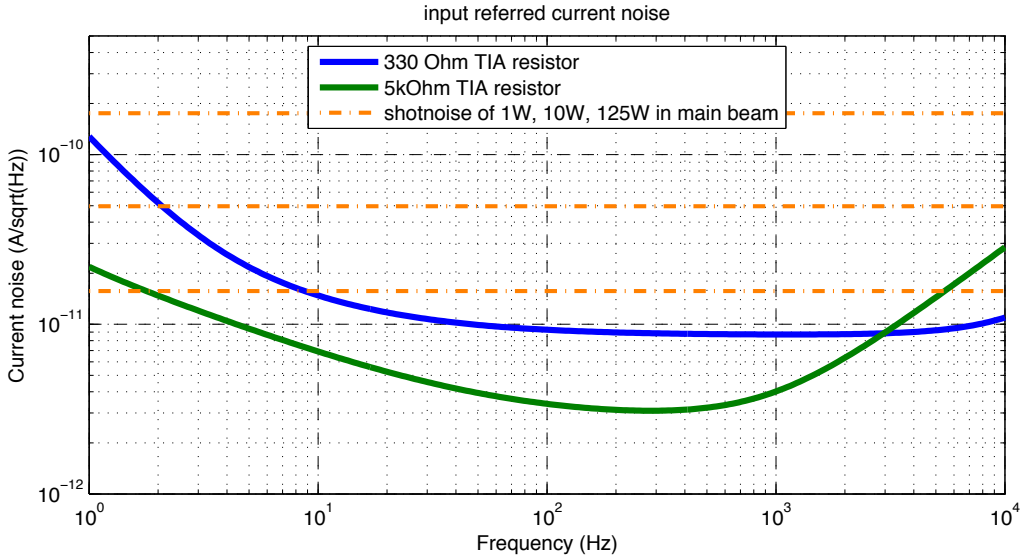

Figure 12: Input referred current noise (LISO simulation)

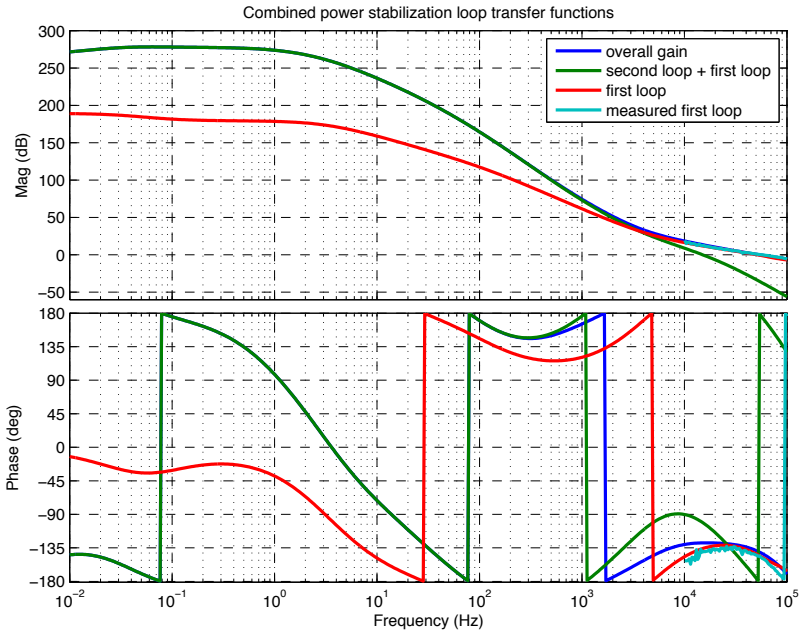

Figure 13: Combined power stabilization loop transfer functions

gain frequency of the is at 50 kHz.

The pole-zero combination at 71.5 mHz, 2.79 Hz and 116.6 Hz is a compensation for the first loop signal conditioning filter. There is a pole at 1 Hz to create a f^{-1} behavior at unity gain and an additional boost (pole at 29 Hz and zero at 808 Hz) to provide additional gain at low frequencies. The zero-pole combination at 4 kHz and 19 kHz is implemented as a pole compensation for the IMC.

A loop test of the analog second loop was done at AEI. Since there is no IMC at the AEI reference system the measurement does not include the IMC filter effect. In addition only one PD from a prototype PD array was used as sensor and the signal conditioning filter has a different behaviour at high frequencies. In the measurement a unity gain frequency of 2 kHz was reached (Fig. 14).

All transfer functions involved in the ISS second loop is shown in figure 15.

4.3.4 Servo loop shape

For a loop with the latter properties a servo design requires poles and zeros as listed in table 2. Furthermore a DC gain of 325 is required. The servo transfer function is drawn in figure 16.

The second loop servo (D1300439) is equipped with an optional integrator which might

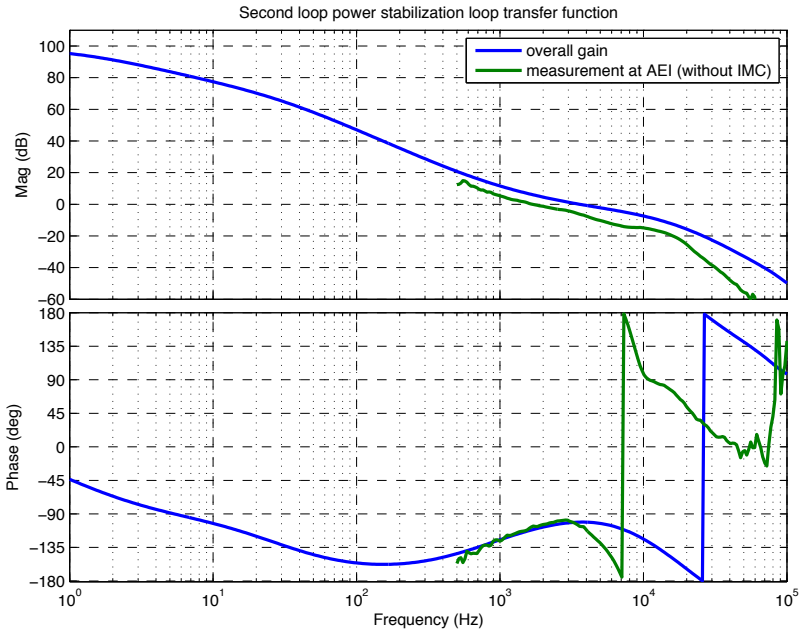

Figure 14: Second loop transfer function

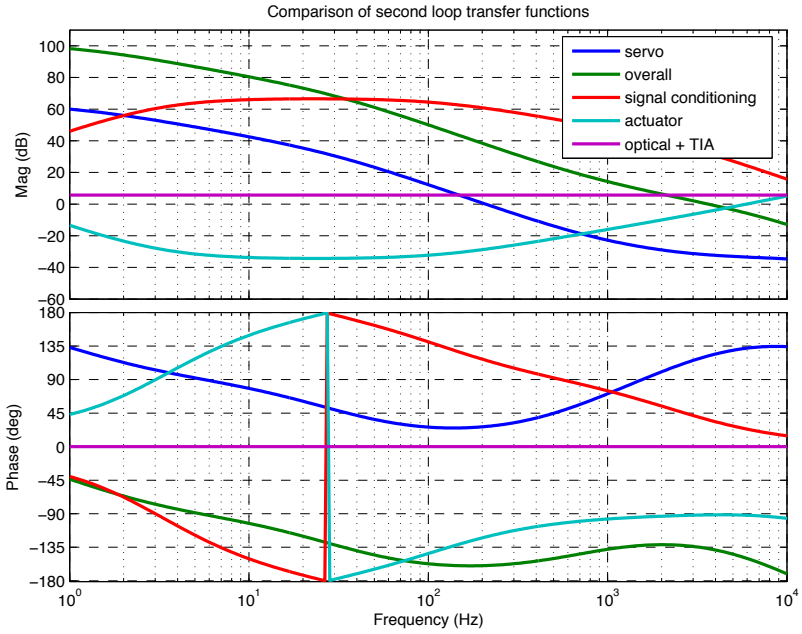

Figure 15: Second loop transfer functions

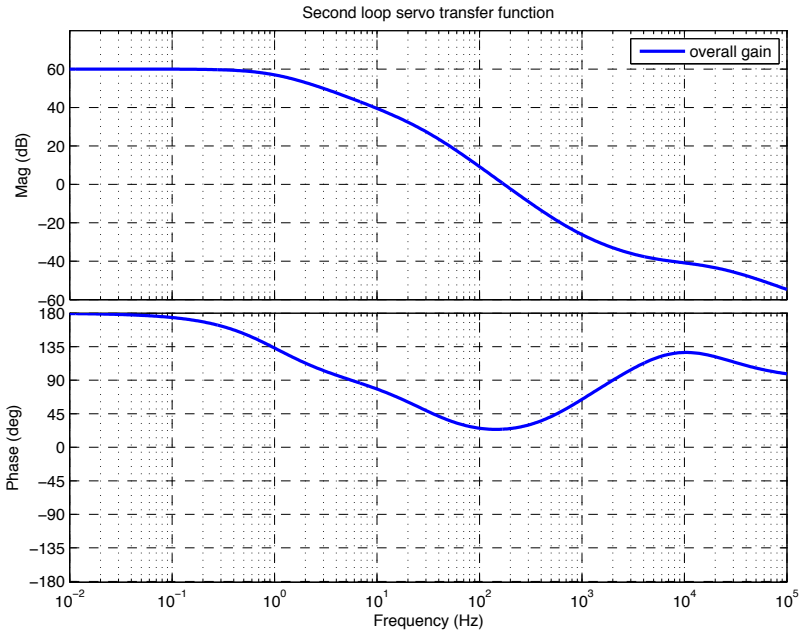

Figure 16: Second loop servo transfer function

be used to stabilize the loop to the DC level detected at the second loop detector. Furthermore, there is a variable DC offset to set the reference level of the loop and a variable gain amplifier.

4.4 Expected noise

The transfer functions derived in the last section were used to estimate the residual power noise on the laser beam that is injected into the interferometer when the second loop power stabilization is enabled. The projections are shown in figure 17. The noise measured in transmission of the IMC was used as worst case scenario. Furthermore, the noise level measured in reflection of the IMC was projected that neglects the pointing to power noise coupling from the IMC. A third noise input is taken from a projection of the IMCs output relative power noise with less contribution of the PZT voltage noise to beam pointing noise coupling as mentioned in LLO alog 6446 (summary on IMC beam jitter).

zero	808 Hz	4030 Hz	
pole	1 Hz	29 Hz	19 kHz
gain	325		

Table 2: Poles and zeros of second loop servo electronics

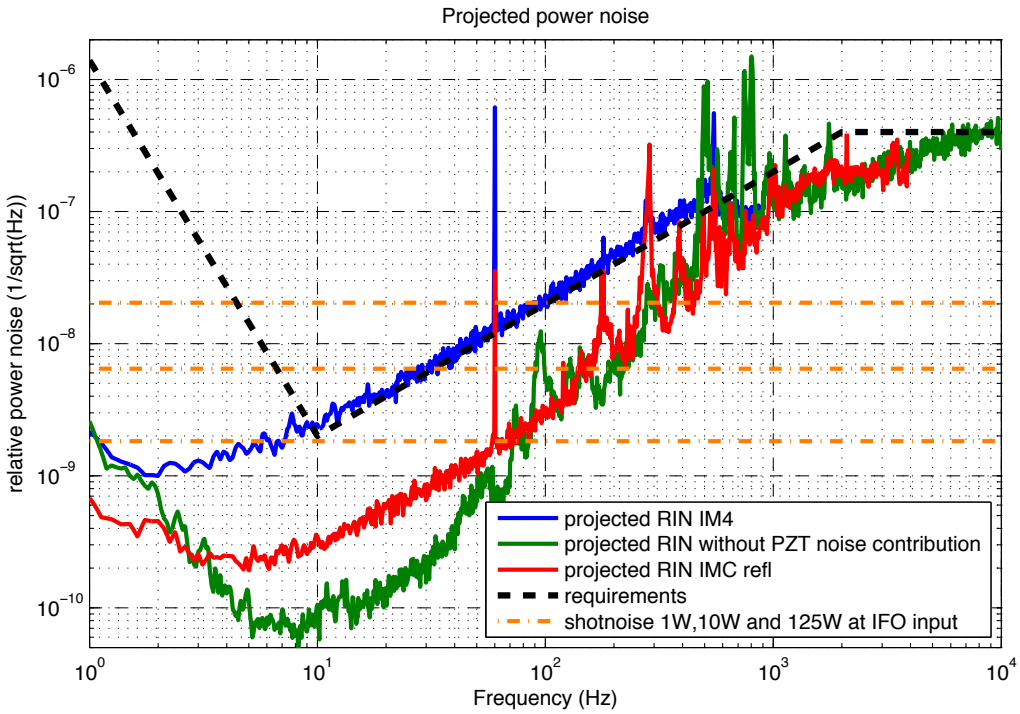

Figure 17: Expected noise suppression and shot noise for various input noises

In two of the three cases the projected noise is below the requirements in the 10-100 Hz band. At higher Fourier frequencies there are some peaks that exceed the requirements which are caused by mechanical resonances of components in the laser room (mainly the IO periscope) and due to vibrations caused by the laser cooling water. However, shot noise contribution will not allow to reach the required power noise level around 10 Hz if the power send towards the interferometer is less than 100 W (Fig.17).

4.5 Saturation effects

It has to be ensured that the signal that is injected into the first loop error point is not causing saturations. To test the robustness of the input, a sine wave was injected and the amplitude was determined at which the first loop was not able to keep the error point close to zero any more (Fig.18).

A power accent increases the actuator gain of the second loop. A similar effect occurs in the first loop and is compensated for via attenuators in the sensing box. For the second loop the effect has to be compensated with the variable gain.

At the error point of the first loop, however, the signal does not change when the power in the main beam is changed, because the absolute level of power noise changes accordingly. In figure 19 the spectrum and the integrated rms of the signal injected to

the first loops error point are shown for the best and worst case of free running power noise. For both cases the signal is well below the saturation limit.

While the second loop is not closed, the signal at the output of the TIA and the conditioning filter were observed (Fig. 20, Fig. 21). For the worst case the signal conditioning filter is saturated. The graphs do not account for the DC level which is assumed to be 10 V at the output of the TIA and 1 V downstream the signal conditioning filter.

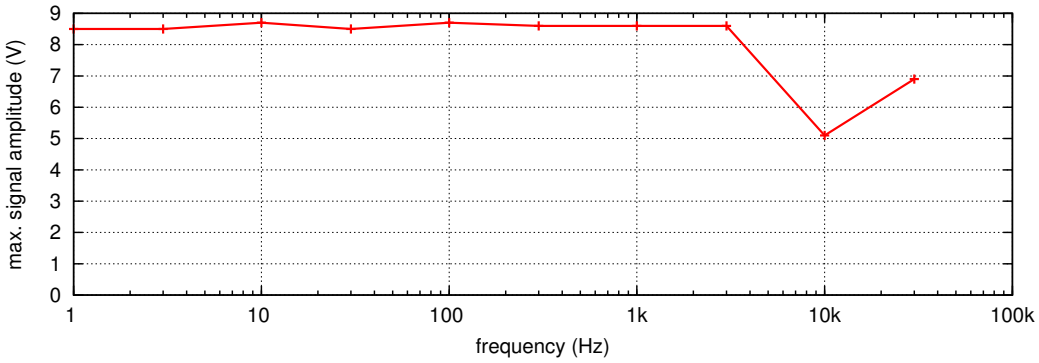

Figure 18: Robustness of first loop error point

4.6 Whitening filter

When the signal of each individual PD is read out by the data acquisition system (DAQ) there is a possibility to add an extra whitening filter. To check if this is actually necessary the anticipated stabilized noise was propagated to the input of the DAQ. The electronics noise of the DAQ input is at the level of $2{\cdot}10^{-6}$ and the expected signal is at least one order of magnitude above this noise level (Fig 22). The dynamic range of the DAQ is more than seven orders of magnitude and therefore the input should not be saturated when the second loop is disabled. Therefore no further whitening is required.

5 Further steps

- update LHO free running power noise measurement
- update free running noise with new cooling circuit configuration
- installation of PD array LHO
- better in-chamber alignment strategy

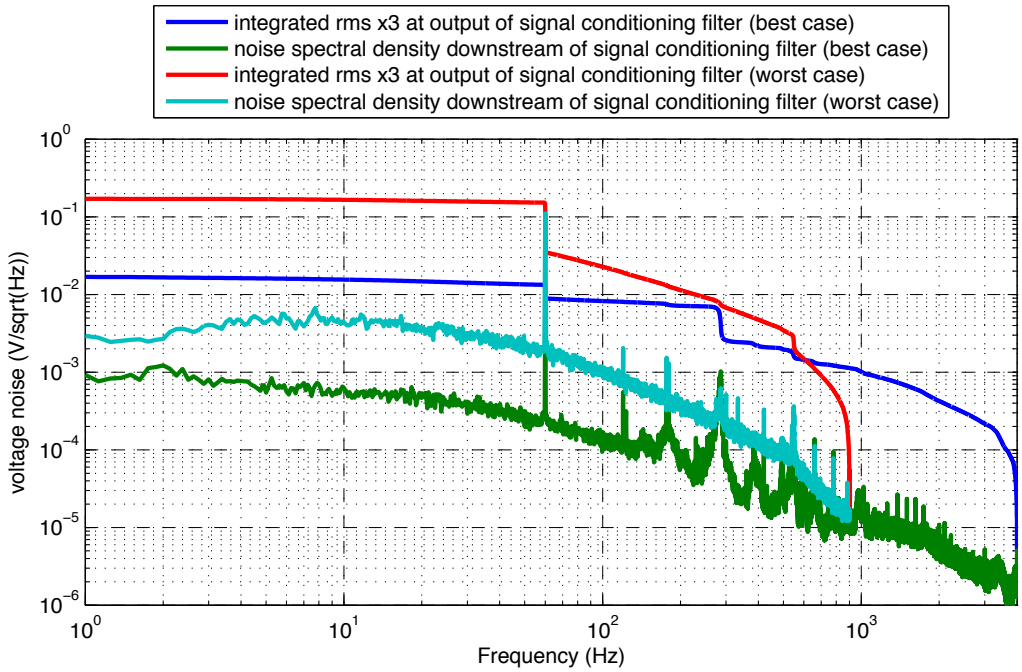

Figure 19: Free running noise propagated to the injection point. The factor of 3 accounts for the peak to peak fluctuations.

- measurement of input referred current noise of readout electronics (with current source)
- add section on RT simulink model for second loop and new channels
- alternative sensors?
- automation
- influence of long in vacuum cables (LLO/LHO comparison)
- include dark current, dark current noise and responsivity measurements of array photo detectors (from Peter)

References

[1] J. Põld. Alignment of ISS PD array and initial testing (LIGO-T1300594). web link

[2] P. Kwee. Laser Characterization and Stabilization for Precision Interferometry. Dissertation. Leibniz Universität Hannover. (2010). web link

[3] P. Kwee, B. Willke, and K. Danzmann. Shot-noise-limited laser power stabilization with a high-power photodiode array. Opt. Lett. 34, 2912-2914 (2009). web link

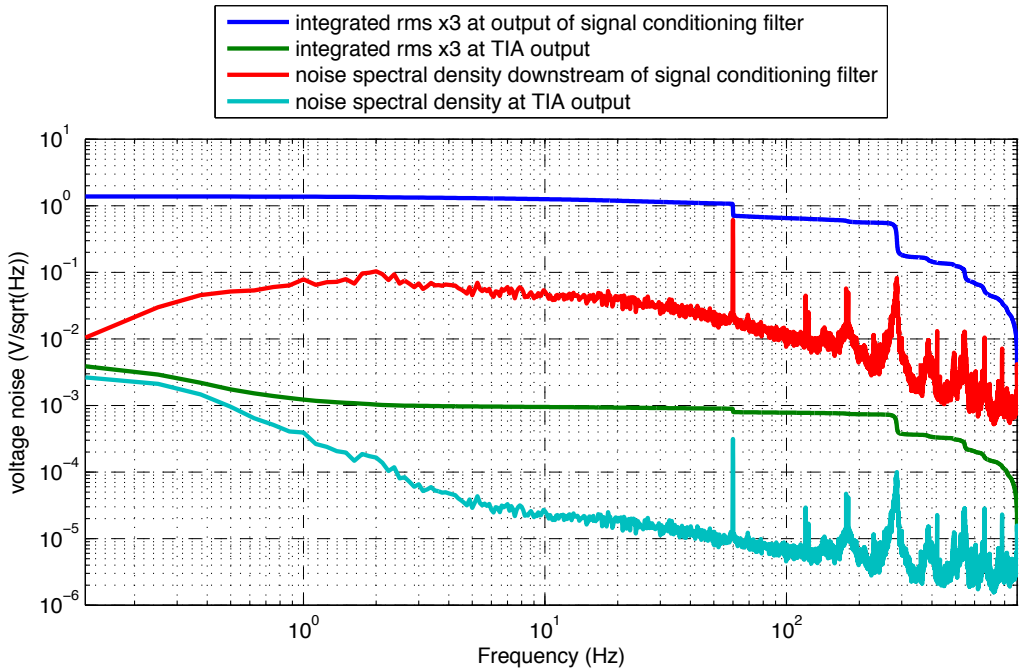

Figure 20: Noise levels at second loop TIA and downstream the signal conditioning filter while the second loop is not closed assuming the noise in reflection of the IMC as input (best case). The factor of 3 accounts for the peak to peak fluctuations.

[4] P. Kwee, C. Bogan, K. Danzmann, M. Frede, H. Kim, P. King, J. Pöld, O. Puncken, R. L. Savage, F. Seifert, P. Wessels, L. Winkelmann, and B. Willke. Stabilized high-power laser system for the gravitational wave detector advanced LIGO. Opt. Express 20. 10617-10634 (2012). web link

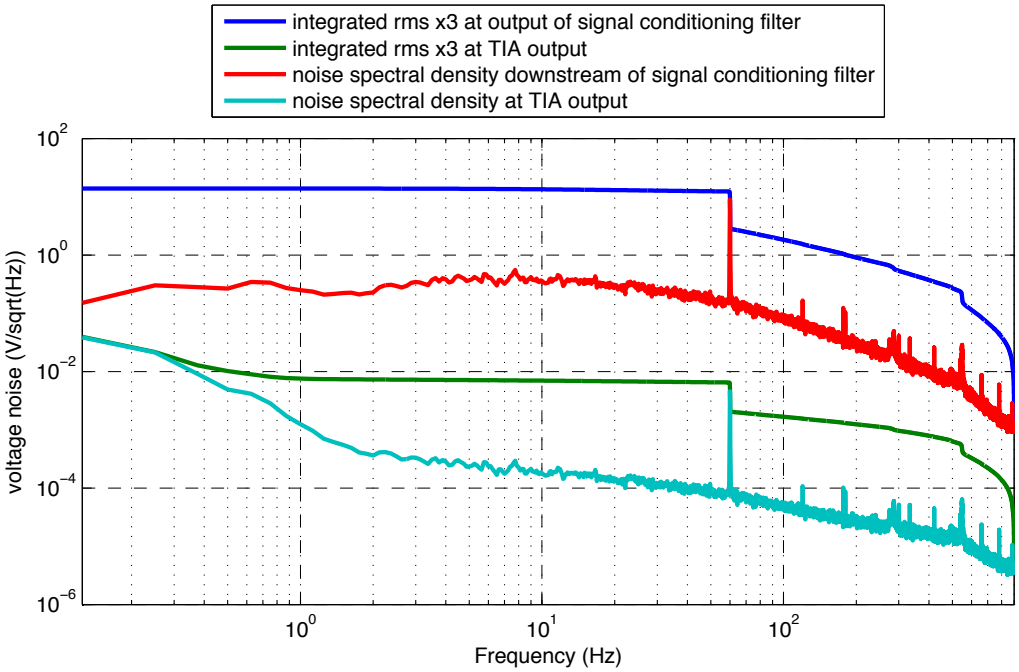

Figure 21: Noise levels at second loop TIA and downstream the signal conditioning filter while the second loop is not closed assuming the noise at IM4 trans as input (worst case). The factor of 3 accounts for the peak to peak fluctuations.

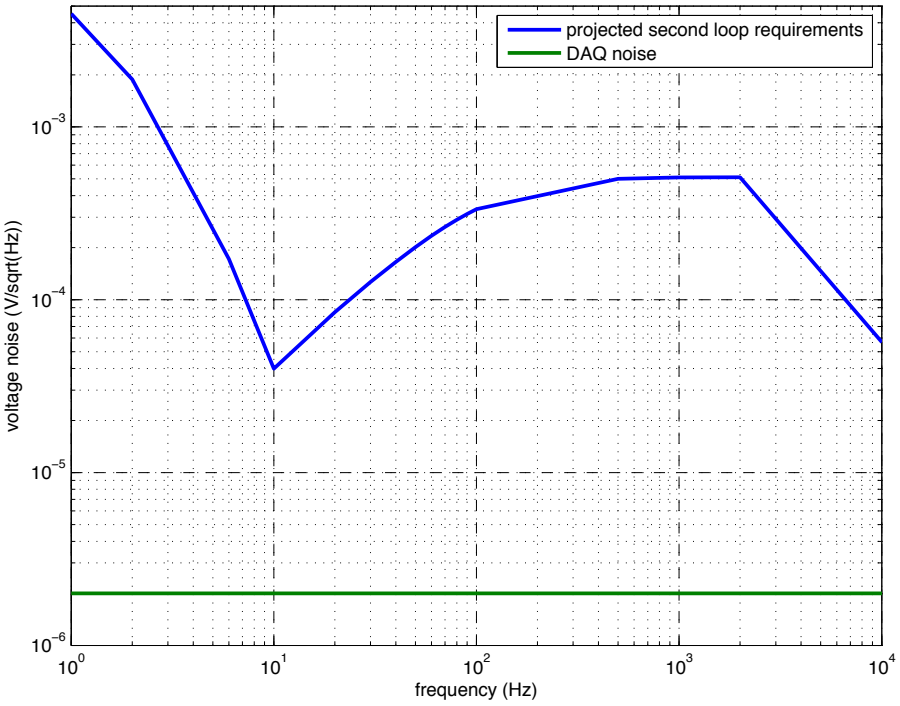

Figure 22: Power noise requirements projected to the input of the DAQ